MOWI®

Hydrodynamic Model Description
Isle of Muck, CAR/L/1109999

February 2022

› Mowi Scotland

OFFICE

PHONE | FAX
-

MAIL

POSTAL

WEB

CONTENTS

LIST OF FIGURES

LIST OF TABLES

1.   Model Description

The hydrodynamic model used in the Muck Azamethiphos Dispersion Modelling Report (Mowi Scotland Ltd., 2022) was RiCOM (River and Coastal Ocean Model), a general-purpose hydrodynamics and transport model, which solves the standard Reynolds-averaged Navier-Stokes equation (RANS) and the incompressibility condition, applying the hydrostatic and Boussinesq approximations. It has been tested on a variety of benchmarks against both analytical and experimental data sets (e.g. Walters & Casulli 1998; Walters 2005a, b). The model has been previously used to investigate the inundation risk from tsunamis and storm surge on the New Zealand coastline (Walters 2005a; Gillibrand et al. 2011; Lane et al. 2011), to study tidal currents in high energy tidal environments (Walters et al. 2010) and, more recently, to study tidal energy resource (Plew & Stevens 2013; Walters et al. 2013; Walters 2016) and the effects of energy extraction on the ambient environment (McIlvenny et al. 2016; Gillibrand et al. 2016).

The basic equations considered here are the three-dimensional (3D) shallow water equations, derived from the Reynolds-averaged Navier-Stokes equations by using the hydrostatic assumption and the Boussinesq approximation. The continuity equation for incompressible flows is:

$$\nabla \cdot u + \frac{\partial w}{\partial z} = 0 \tag{1}$$

where u(x,y,z,t) is the horizontal velocity vector, w(x,y,z,t) is the vertical velocity, ∇ is the horizontal gradient operator, and z is the vertical coordinate. The momentum equation in non-conservative form is given by:

$$\frac{Du}{Dt} + f\hat{z} \times u + \frac{1}{\rho_0}\nabla p - \frac{\partial}{\partial z}\left(A_V \frac{\partial u}{\partial z}\right) - \nabla \cdot (A_h \nabla u) + F = 0 \tag{2}$$

where t is time; f(x,y) is the Coriolis parameter; $\hat{z}$ is the upward unit vector; p(x,y,z,t) is pressure; ρ_0 is a reference density; A_V(x,y,z,t) and A_h(x,y,z,t) are the vertical and horizontal eddy viscosities respectively; F represents body forces including form drag from obstacles in the flow; and x, y are the horizontal coordinates aligned to the east and north respectively.

The free surface equation is formed by vertically integrating the continuity equation and applying the kinematic free surface and bottom boundary conditions:

$$\frac{\partial \eta}{\partial t} - \nabla \cdot \left(\int_{-H}^{\eta} u dz\right) = 0 \tag{3}$$

where H is the water depth relative to the mean level of the sea.

The model can be run in two- or three-dimensional mode. Frictional stress, τ_b, is applied at the seabed as a quadratic function of velocity:

$$\tau_b = \rho C_D U_b |U_b| \tag{4}$$

where ρ = 1025 kg m^{-3} is the water density. The velocity, U_b, is either the velocity at the lowest sigma layer if the model is run in 3D or the depth-averaged velocity if run in 2D. The drag coefficient, C_D, can be either a constant or calculated from the bed roughness lengthscale, z_0, using:

$$C_D = \left(\frac{\kappa}{\ln \left((z_b + z_0)/z_0 \right)} \right)^2 \qquad (5)$$

where κ=0.4 is von Karman's constant, and z_b is the height above the bed of the lowest velocity point.

Wind forcing was applied as a surface stress calculated from hourly wind speed and direction. Wind stress was calculated from the wind velocity by a standard quadratic relation:

$$\tau_x = \rho_a C_S u W \qquad (6a)$$
$$\tau_y = \rho_a C_S v W \qquad (6b)$$

where (u,v) are the East and North components of wind velocity respectively, W is the wind speed (W = $[u^2+v^2]^{1/2}$), ρ_a is the density of air, and the surface drag coefficient C_S is calculated following Wu (1982) or Large and Pond (1981).

The equations are discretized on an unstructured grid of triangular elements which permits greater resolution of complex coastlines. The momentum and free surface equations are solved using semi-implicit techniques to optimize solution time and avoid the CFL stability constraint (Walters 2016). The material derivative in (2) is discretized using semi-Lagrangian methods to remove stability constraints on advection (Casulli, 1987; Walters et al. 2008). The Coriolis term is solved using a 3rd order Adams-Bashforth method (Walters et al. 2009). Full details of the model discretization and solution methods can be found in Walters et al. (2013) and Walters (2016). The solution methods provide a fast, accurate and robust code that runs efficiently on multi-core desktop workstations with shared memory using OpenMP. Full details of the model discretization and solution methods, including the basis of the application to tidal energy, are given by Walters et al. (2013) and Walters (2016).

2.   Configuration and Boundary Forcing for Muck

The unstructured mesh used in the modelling was adapted from the mesh used by Gillibrand et al. (2016) (Figure 1). This domain was chosen so that the open boundary would be further away from the site of interest than is the case with the Marine Scotland ECLH and WLLS domains. Model resolution was enhanced in the Small Isles region, particularly around the Mowi site at Muck (Figure 2). The spatial resolution of the model varied from 25m in some inshore waters to 20km along the open boundary. The model consisted of 119,925 nodes and 231,016 triangular elements. Bathymetry was taken from the European Marine Observation and Data Network (EMODnet).

The model was forced at the outer boundaries by eight tidal constituents (O_1, K_1, P_1, Q_1, M_2, S_2, N_2, K_2) which were taken from the Scottish Shelf Model (Marine Scotland, 2016). Spatially- and temporally-varying wind speed and direction data were taken from the ERA5 global reanalysis dataset (ECMWF, 2021) for the required simulation periods.
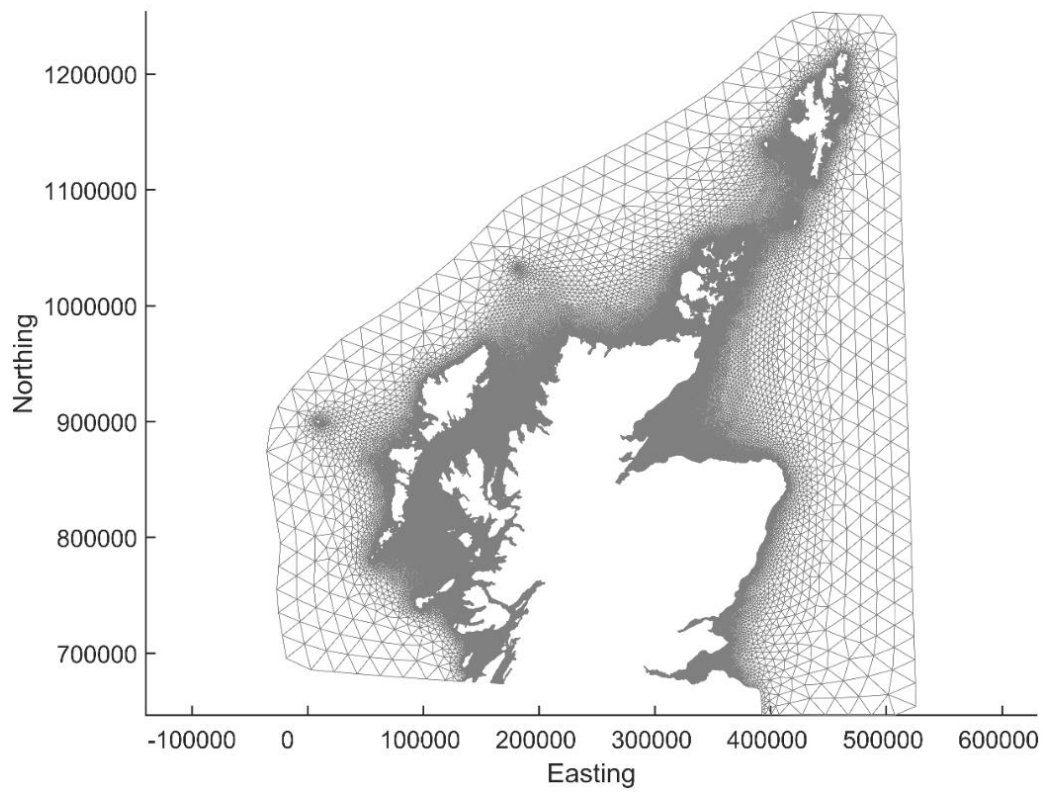
Figure 1. The mesh and domain of the modelling study, adapted from Gillibrand et al (2016)
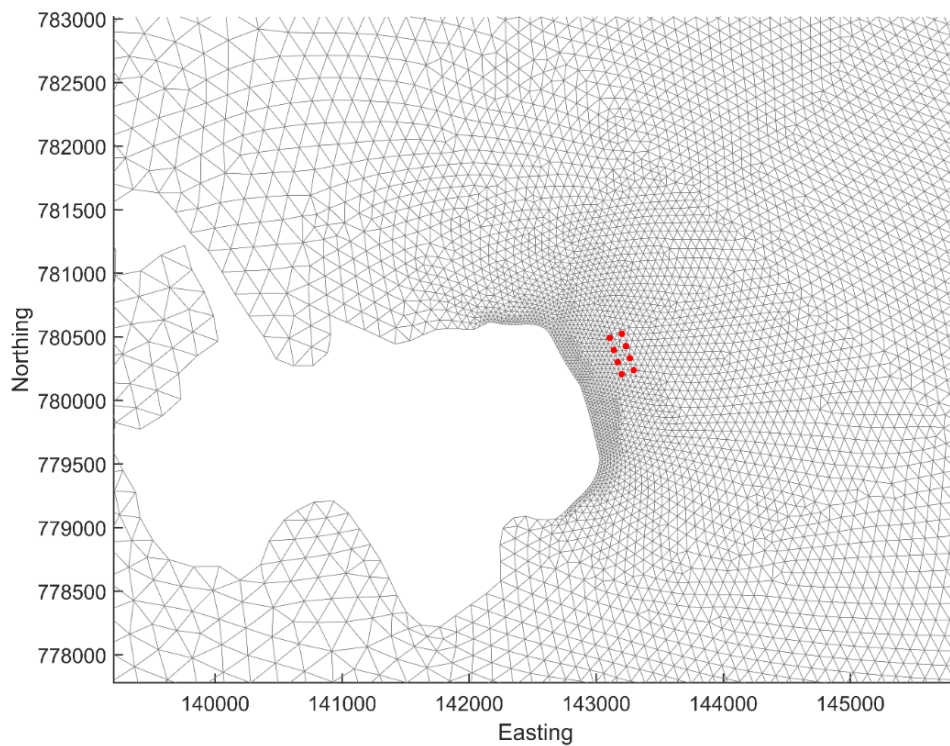
Figure 2. The unstructured mesh around the Muck site in the modified model grid, with the proposed cage locations indicated (•).
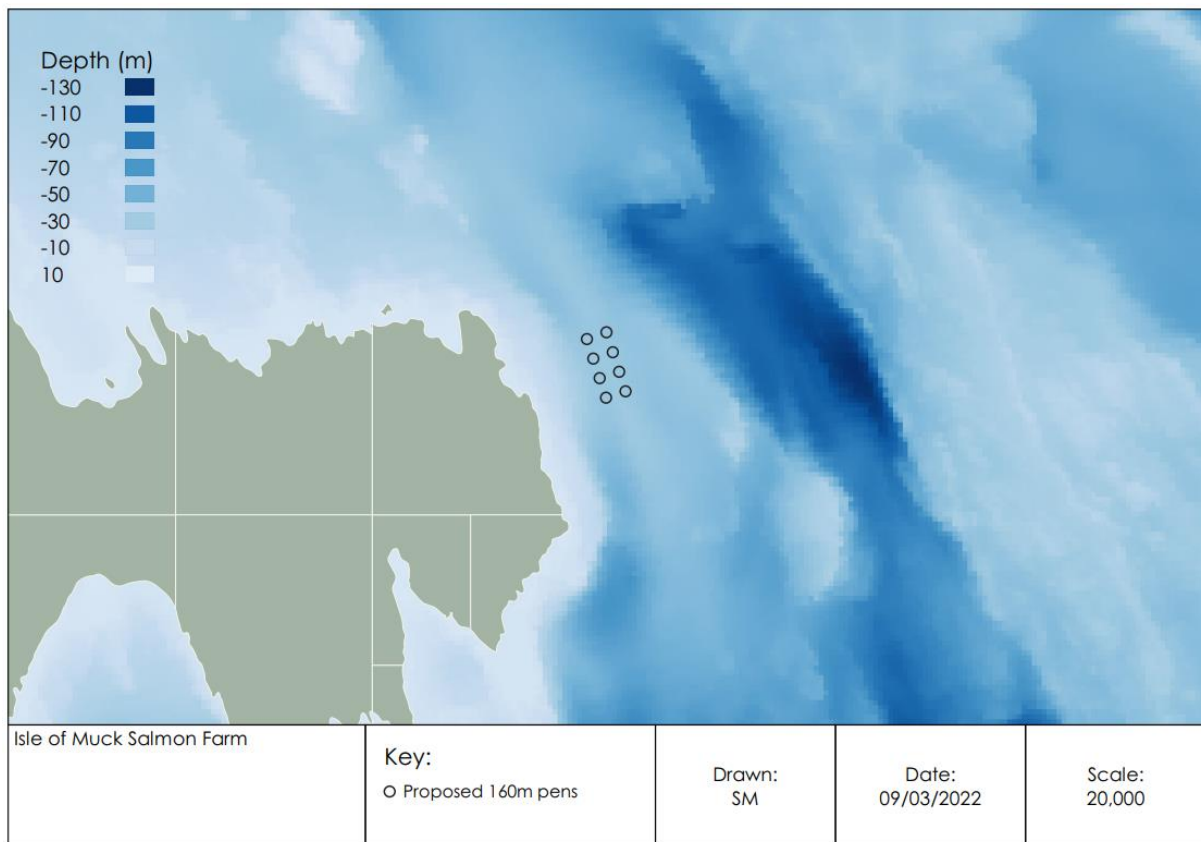
Figure 3. Model water depths (m) in the area around Muck salmon farm.

3.   Model Calibration and Validation

The RiCOM model has previously been calibrated against sea level and current meter data from the north of Scotland (Gillibrand et al. 2016). For the current study, the model was further calibrated against hydrographic data collected in the region of the farm site in 2010 and again in 2021. The data are described in the relevant hydrographic reports. In April 2010, two Workhorse Acoustic Doppler Current Profilers (ADCPs) were deployed close to the farm site (Figure 4) until May 2010 (ID350 & ID351). In January 2021, another ADCP was deployed close to the farm site (Figure 4) until April 2021 (ID366). In all, 157 days of current data were used in this application. ADCP deployments provided both current velocity and seabed pressure data, which were used to calibrate and validate modelled velocity and sea surface height. The model was calibrated initially against data from April – May 2010 (ID350), then validated against data from the other two deployments, ID351 and ID366 from 2010 and 2021 respectively.

For each simulation, the model was "spun-up" for three days with boundary forcing ramped up from zero over a period of 48 hours. The model state at the end of the 72-hour spin-up period was stored, and the main simulations "hot-started" from this state.

The following main simulations were performed, corresponding with the dates of the ADCP deployments:

(i)   Calibration: 8th April 2010 – 19th May 2010 (ID350)
(ii)   Validation: 8th April 2010 – 18th May 2010 (ID351)
(iii)   Validation: 27th January – 15th April 2021 (ID366)

[Note that the dates above refer to the main simulations and that the spin-up simulations ran for three days prior to the start dates given above.]
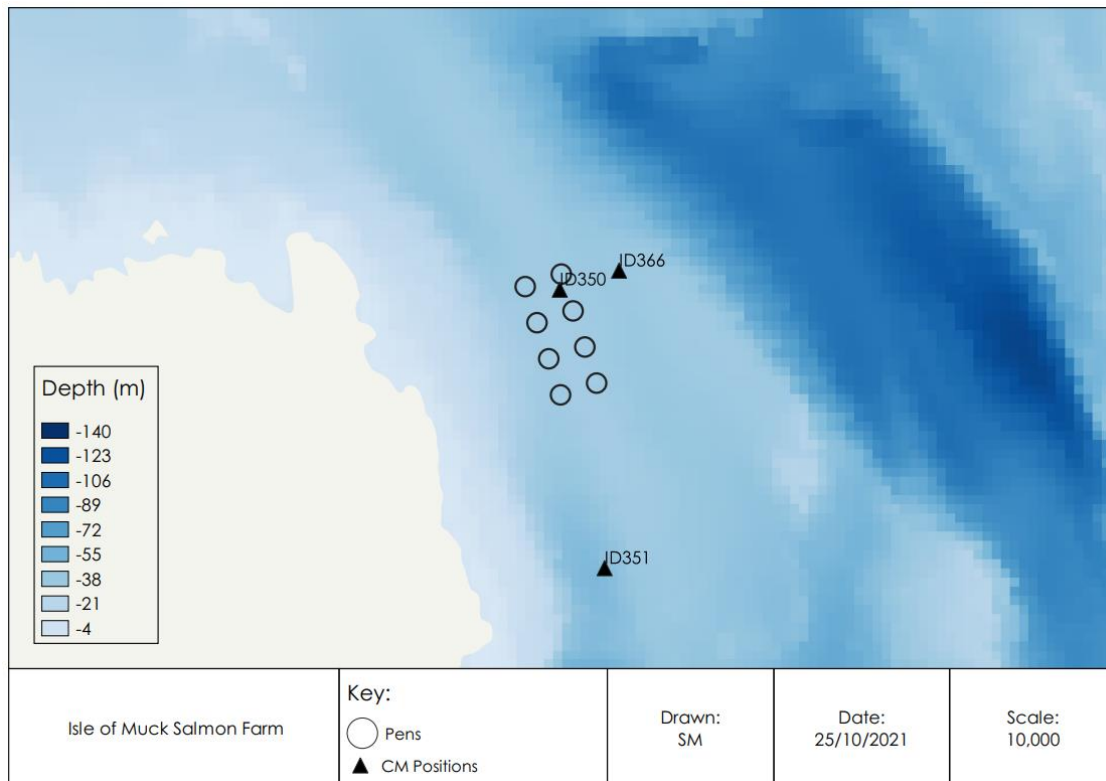
Figure 4. Locations of the ADCP deployments relative to the proposed 8 pens at the Isle of Muck site.

Model performance is assessed using three metrics: the mean absolute error (MAE), the root-mean-square error (RMSE) and the model skill (d_2). The first two are standard measures of model accuracy; the third, d_2, is taken from Willmott et al. (1985) and lies in the range $0 \leq d_2 \leq 1$, with $d_2 = 0$ implying zero model skill and $d_2 = 1$ indicating perfect skill.

3.1   Calibration: April – May 2010, ID350

The calibration used observed depth and current velocity from the ADCP location to compare with modelled sea surface height (SSH) and velocity (ADCP deployment ID350). The model was calibrated by varying the value of the drag coefficient, C_D, in Equation A4, which determines the frictional effect of the seabed on the flow. Simulations were performed with a range of values of C_D, varying over the range $0.002 \leq C_D \leq 0.02$. After a number of simulations, a final parameter set was selected (Table 1).

Table 1. Parameter values chosen for the RiCOM model during the calibration simulations.

Parameter Description	Value
Drag coefficient, C_D	0.002
Number of vertical levels	1
Model time step (s)	72

The results of the calibration exercise are presented in Figure 5 – Figure 8 and Table 2. At the ADCP location, the sea surface height was reasonably accurately modelled, with model skill of 0.91. The mean absolute error (MAE) and root-mean-square error (RMSE) values of 0.51 m and 0.62 respectively are about 12.37 % and 15.03 % of the spring tide range respectively.

For the calibration period, the model skill scores were 0.62 and 0.80 for the East and North components of velocity respectively. RMSE values were 0.06 m s^{-1} and 0.12 m s^{-1} for the two components of velocity (Table 2). The scatter plots and histograms demonstrate that the modelled current had broadly the same magnitude and direction characteristics as the observed data (Figure 7 and Figure 8).
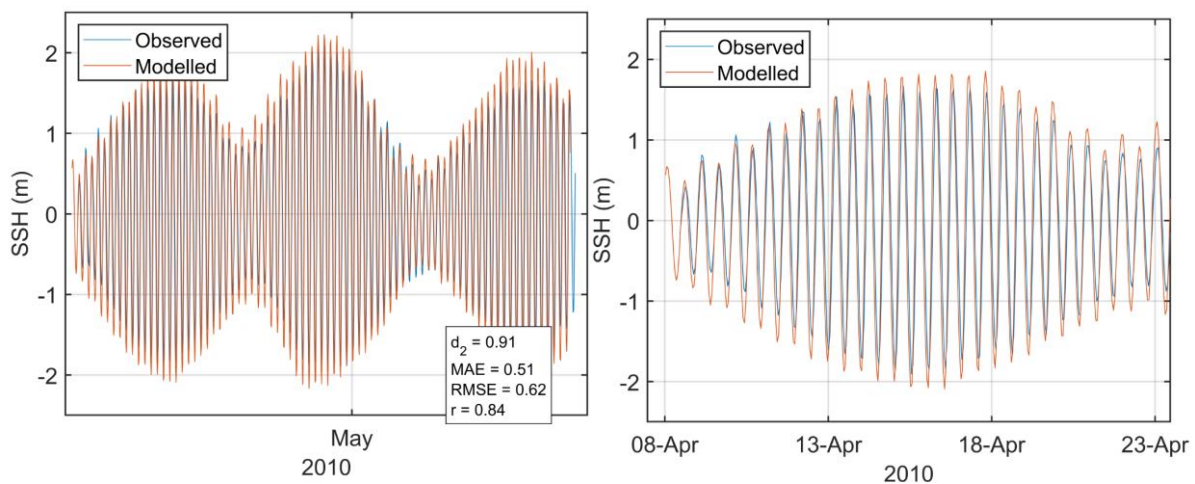
Figure 5. Comparison between observed and modelled sea surface height from April – May 2010 (ADCP deployment ID350) using model parameter values from Table 1. Both the full record (left) and a subset of 15 days (right) are shown. Observed data are in blue, model results in red.

Table 2. Model performance statistics for sea surface height (SSH) and East and North velocity at the ADCP location from April – May 2010 (ID350).

	SSH	East	North
Model skill, d_2	0.91	0.62	0.80
Mean Absolute Error (MAE)	0.51 m	0.05 m s^{-1}	0.11 m s^{-1}
Root-Mean-Square Error (RMSE)	0.62 m	0.06 m s^{-1}	0.12 m s^{-1}

Figure 6. Comparison between observed and modelled East (top) and North (bottom) components of velocity at the ADCP location for 15 days in April - May 2010 (ID350). Observed data are in blue, model results in red.
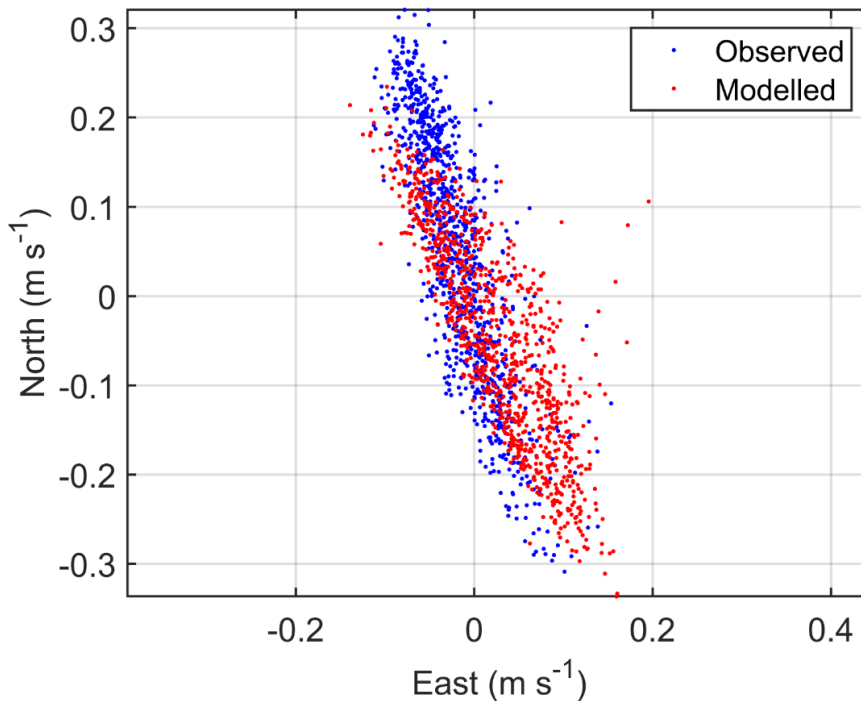
Figure 7. Scatter plot of observed and modelled velocity at the ADCP location from April – May 2010 (ID350). Observed data are in blue, model results in red.
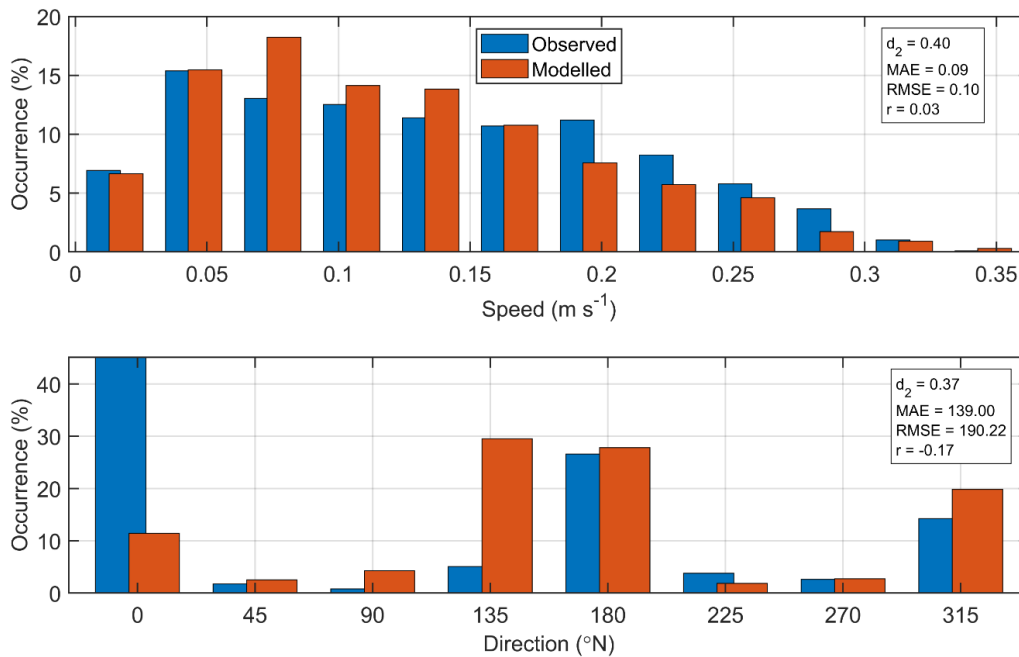
Figure 8. Histograms of observed and modelled speed (top) and direction (bottom) at the ADCP location from April – May 2010 (ID350). Observed data are in blue, model results in red.

3.2   Validation: April – May 2010, ID351

At the ADCP location, the sea surface height was reasonably accurately modelled, with model skill of 0.95 (Figure 9, Table 3). The mean absolute error (MAE) and root-mean-square error (RMSE) values of 0.37 m and 0.45 m respectively are about 9.0 % and 10.9 % of the spring tide range respectively.

North and east components of velocity at the ADCP location were satisfactorily reproduced by the model, with values of the model skill, d_2, of about 0.88 and 0.60 respectively (Figure 10, Table 3). The values of the MAE and RMSE being in the range 2 – 12 cm s^{-1} (Table 3). The scatter plots and histograms shown in Figure 11 and Figure 12 demonstrate that the modelled currents were broadly of the same speed and direction as the observed data.

Table 3. Model performance statistics for sea surface height (SSH) and East and North velocity at the ADCP location from April – May 2010 (ID351).

|	SSH	East	North
Skill, d_2	0.95	0.60	0.88
Mean Absolute Error (MAE)	0.37 m	0.02 m s^{-1}	0.10 m s^{-1}
Root-Mean-Square Error (RMSE)	0.45 m	0.02 m s^{-1}	0.12 m s^{-1}

Figure 9. Comparison between observed and modelled sea surface height from April – May 2010 (ADCP deployment ID351) using model parameter values from Table 1. Both the full record (left) and a subset of 15 days (right) are shown. Observed data are in blue, model results in red.
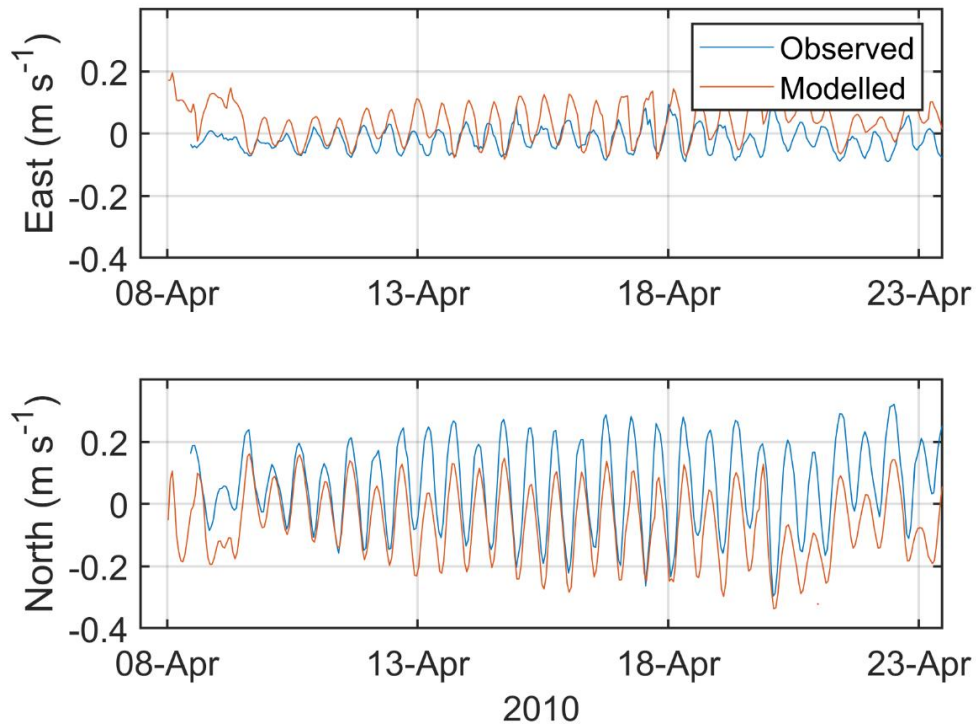

Figure 10. Comparison between observed and modelled East (top) and North (bottom) components of velocity at the ADCP location for 15 days in April – May 2010 (ID351). Observed data are in blue, model results in red.
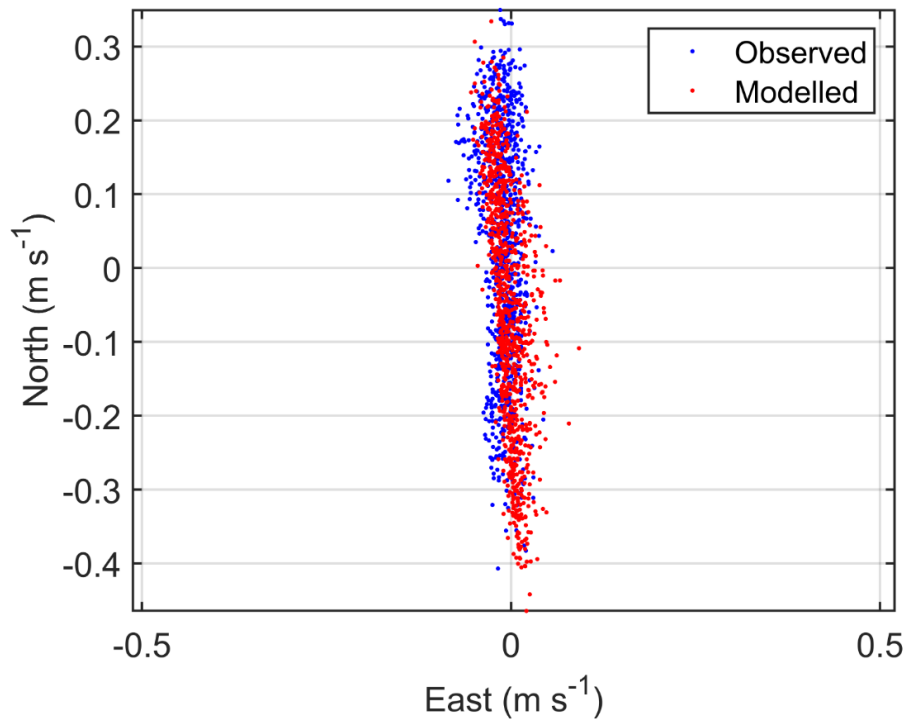
Figure 11. Scatter plot of observed and modelled velocity at the ADCP location from April – May 2010 (ID351). Observed data are in blue, model results in red.
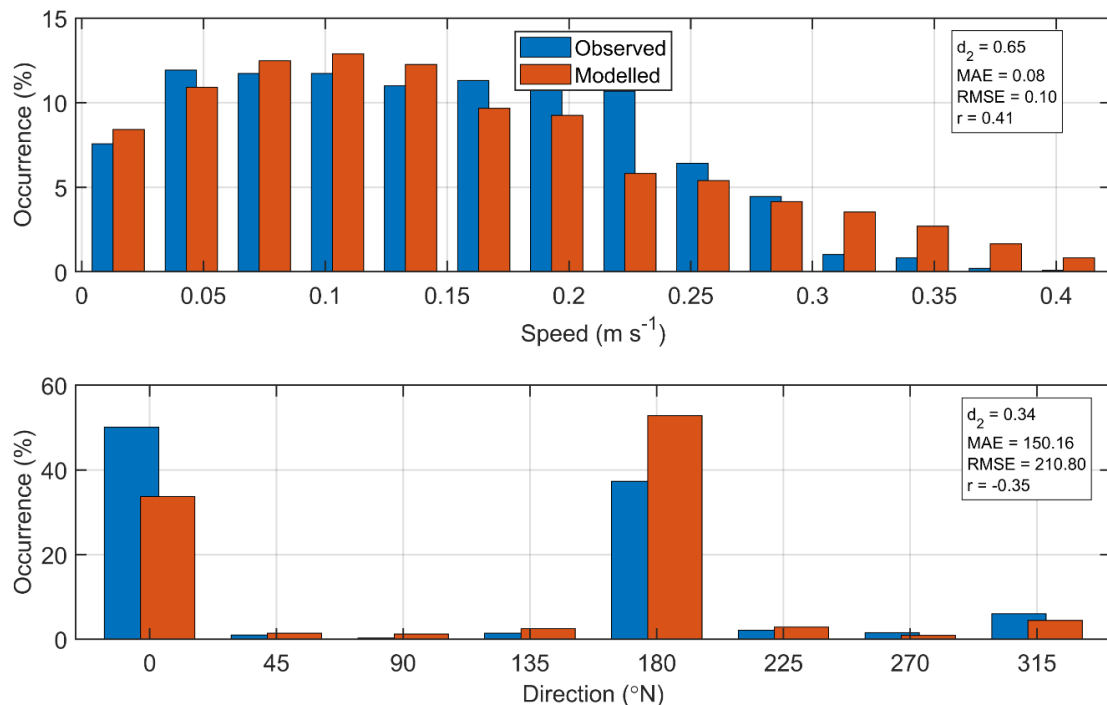
Figure 12. Histograms of observed and modelled current speed (top) and direction (bottom) at the ADCP location from April – May 2010 (ID351). Observed data are in blue, model results in red.

3.3   Validation: January – April 2021, ID366

At the ADCP location, the sea surface height was reasonably accurately modelled, with model skill of 0.99 (Figure 13, Table 4). The mean absolute error (MAE) and root-mean-square error (RMSE) values of 0.18 m and 0.23 respectively are about 3.61 % and 4.61 % of the spring tide range respectively.
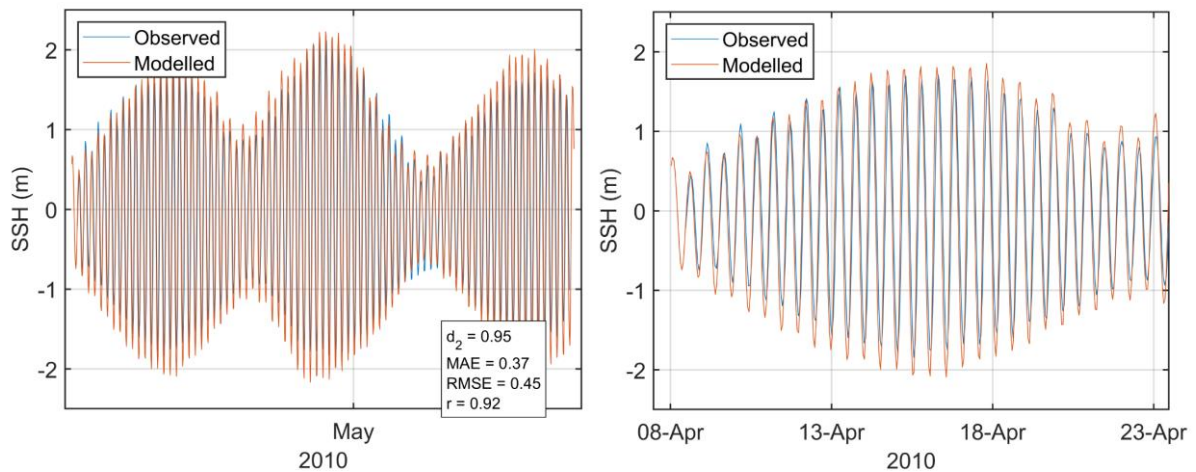

Figure 13. Comparison between observed and modelled sea surface height from January – April 2021 (ADCP deployment ID366) using model parameter values from Table 1. Both the full record (left) and a subset of 15 days (right) are shown. Observed data are in blue, model results in red.
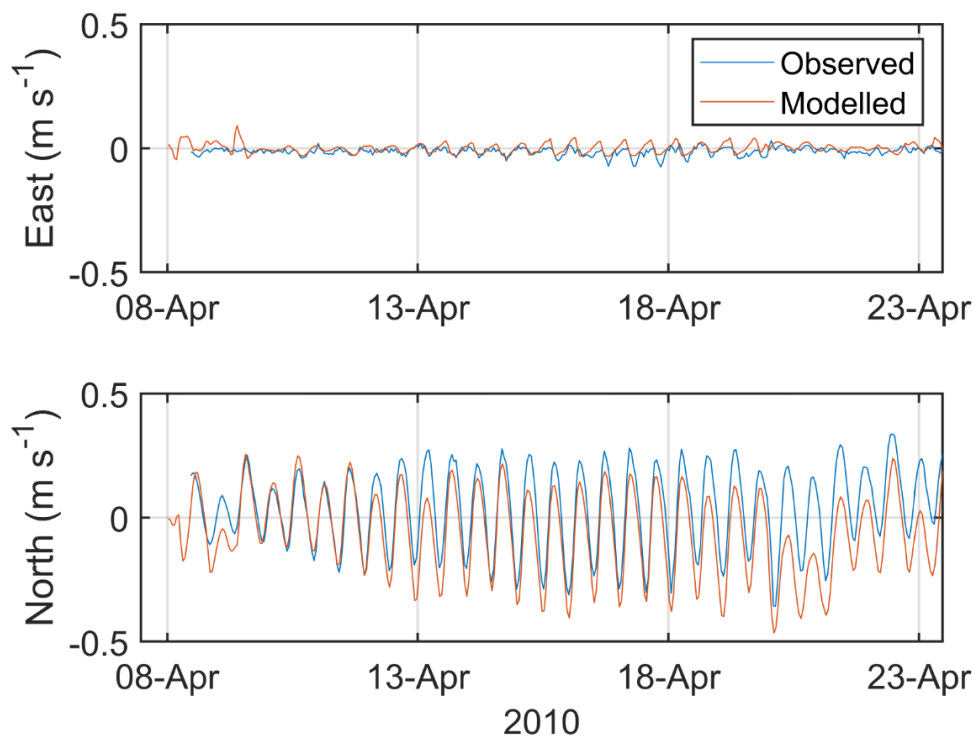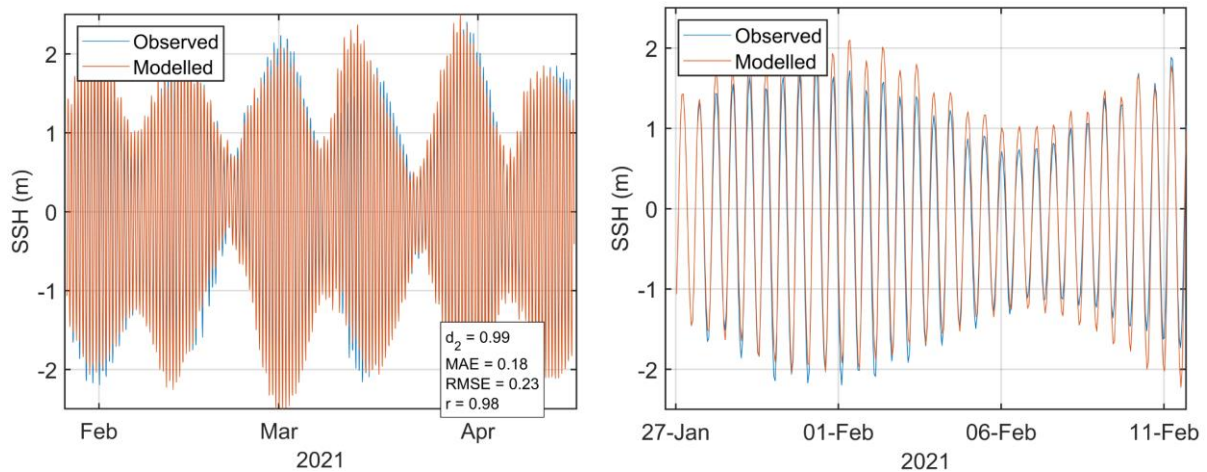
North and east components of velocity at the ADCP location were satisfactorily reproduced by the model, with values of the model skill, d_2, of 0.68 and 0.45 of velocity (Figure 14, Table 4). The values of the MAE and RMSE were in the range 5 - 16 cm s^{-1} (Table 4). The histograms ((Figure 15) demonstrate that the modelled currents were broadly of the same speed and direction as the observed data.

However, the scatter plot (Figure 16) indicates that the modelled velocities were somewhat misaligned with the observed data. We have explored this, and extracted modelled velocity data from nearby cells for comparison with the observations; the rationale here is that deployment of current meters in fast-flowing currents may result in the actual current meter location being offset compared to the nominal location. However, for all neighbouring model cells, the directional offset between observed and modelled data persisted. We therefore think it likely that the ADCP was deployed close to a relatively small-scale bathymetric feature that was not captured in the model bathymetry. The good agreement between modelled and observed data from nearby ID350 supports this case, since it is the observed data from ID366 that are offset relative to ID350, whereas the modelled results exhibit the same general orientation. We therefore believe that the general circulation around Muck simulated by the model is acceptable despite this localised anomaly.

Table 4. Model performance statistics for sea surface height (SSH) and East and North velocity at the ADCP location from January – April 2021 (ID366).

	SSH	East	North
Skill, d_2	0.99	0.45	0.68
Mean Absolute Error (MAE)	0.18 m	0.05 m s^{-1}	0.13 m s^{-1}
Root-Mean-Square Error (RMSE)	0.23 m	0.06 m s^{-1}	0.16 m s^{-1}

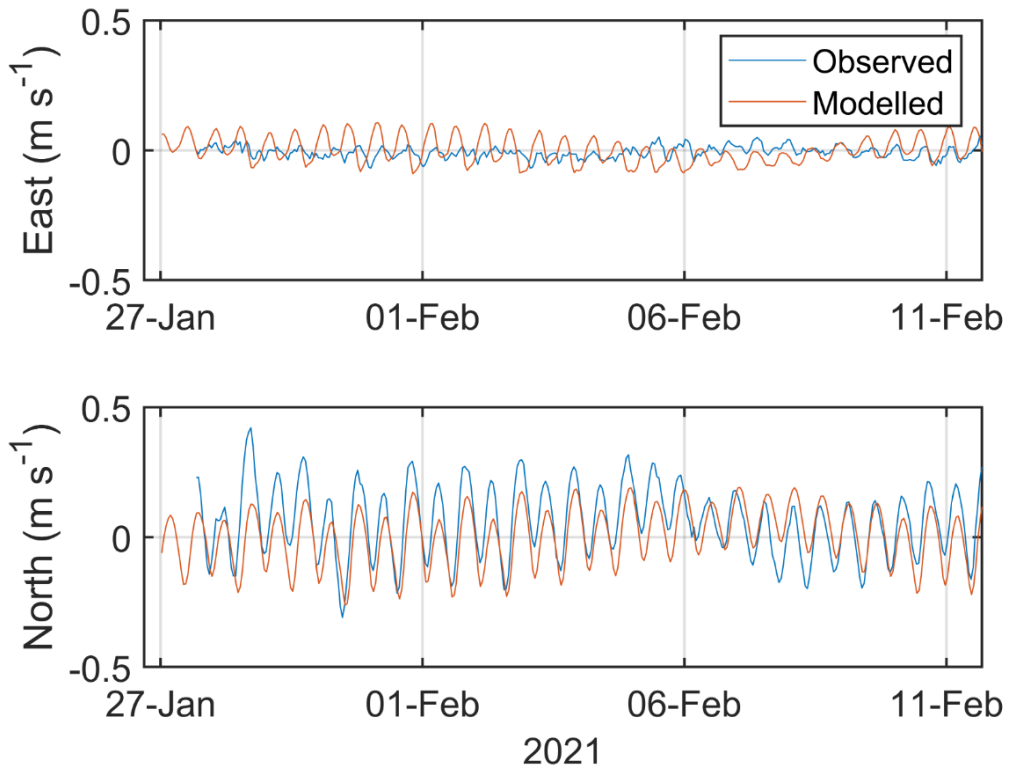*Figure 14. Comparison between observed and modelled East (top) and North (bottom) components of velocity at the ADCP location for 15 days in January – April 2021 (ID366). Observed data are in blue, model results in red.*
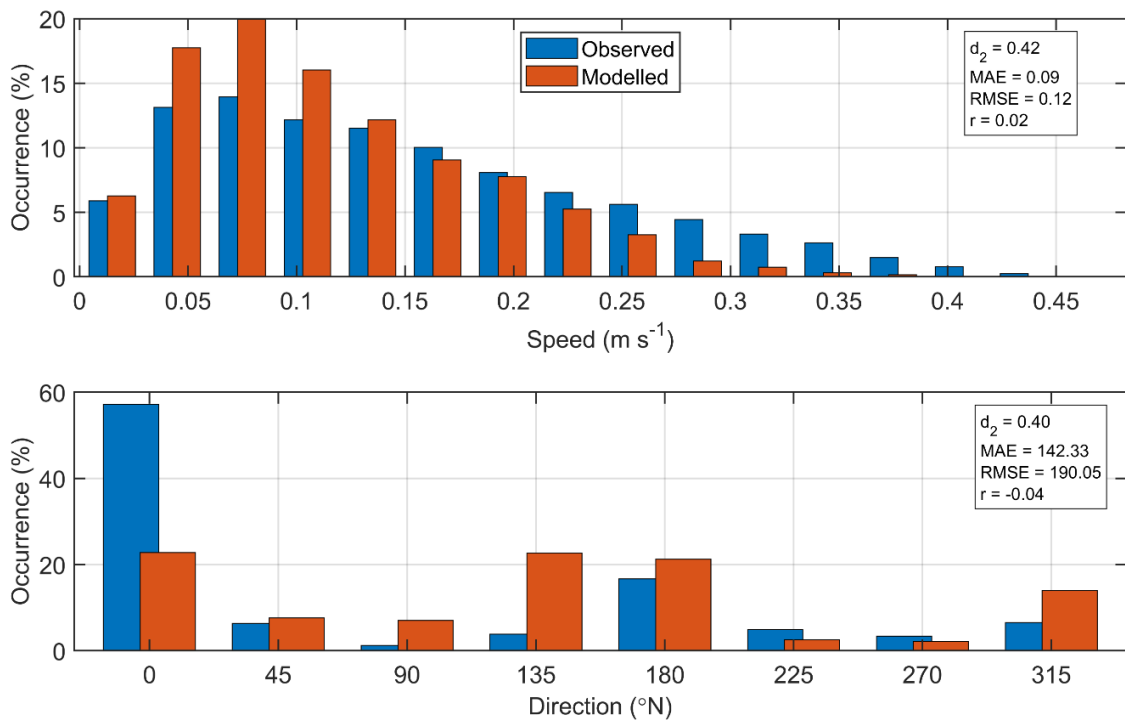

Figure 15. Histograms of observed and modelled current speed (top) and direction (bottom) at the ADCP location from January – April 2021 (ID366). Observed data are in blue, model results in red.
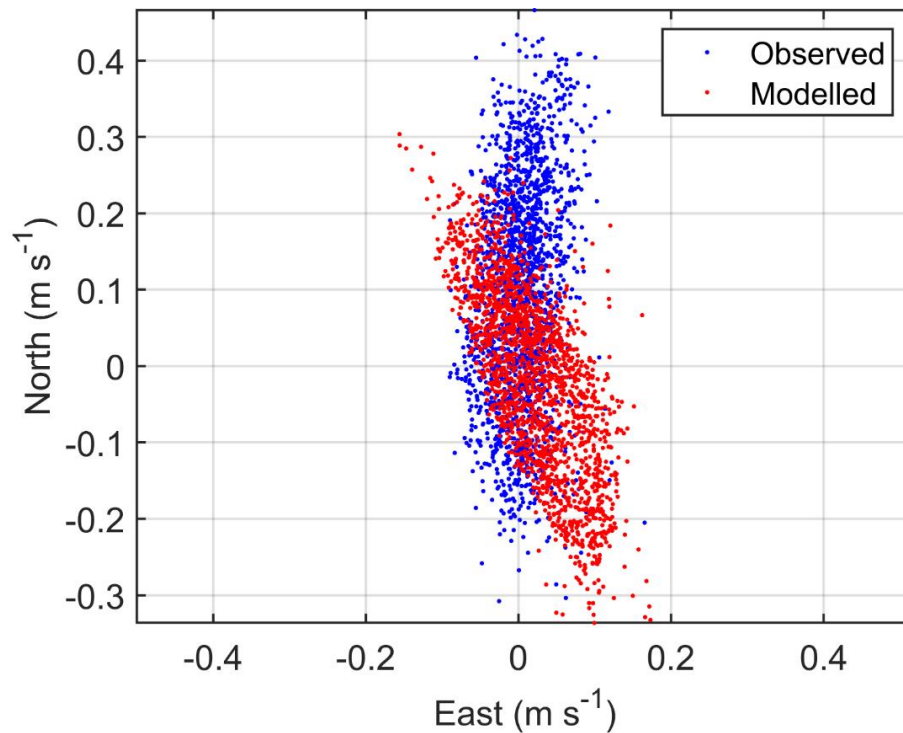
Figure 16. Scatter plot of observed and modelled velocity at the ADCP location from January – April 2021 (ID366). Observed data are in blue, model results in red.

4.   Modelled Flow Fields

Modelled flood and ebb velocity vectors at spring tides are illustrated in Figure 17. The Muck site is exposed to the strong currents from around the Ardnamurchan peninsula. The prevailing flow is north-westwards which is typical of the Scottish Coastal Current. Currents are strong around the Muck site, with a mean near-surface speed exceeding 0.15 m s^{-1}.

Figure 17. Modelled flood (top) and ebb (bottom) surface current vectors during spring tides on 28th April 2010 and 29th April 2010 respectively. For clarity, only every 10th element of the model vectors are shown.
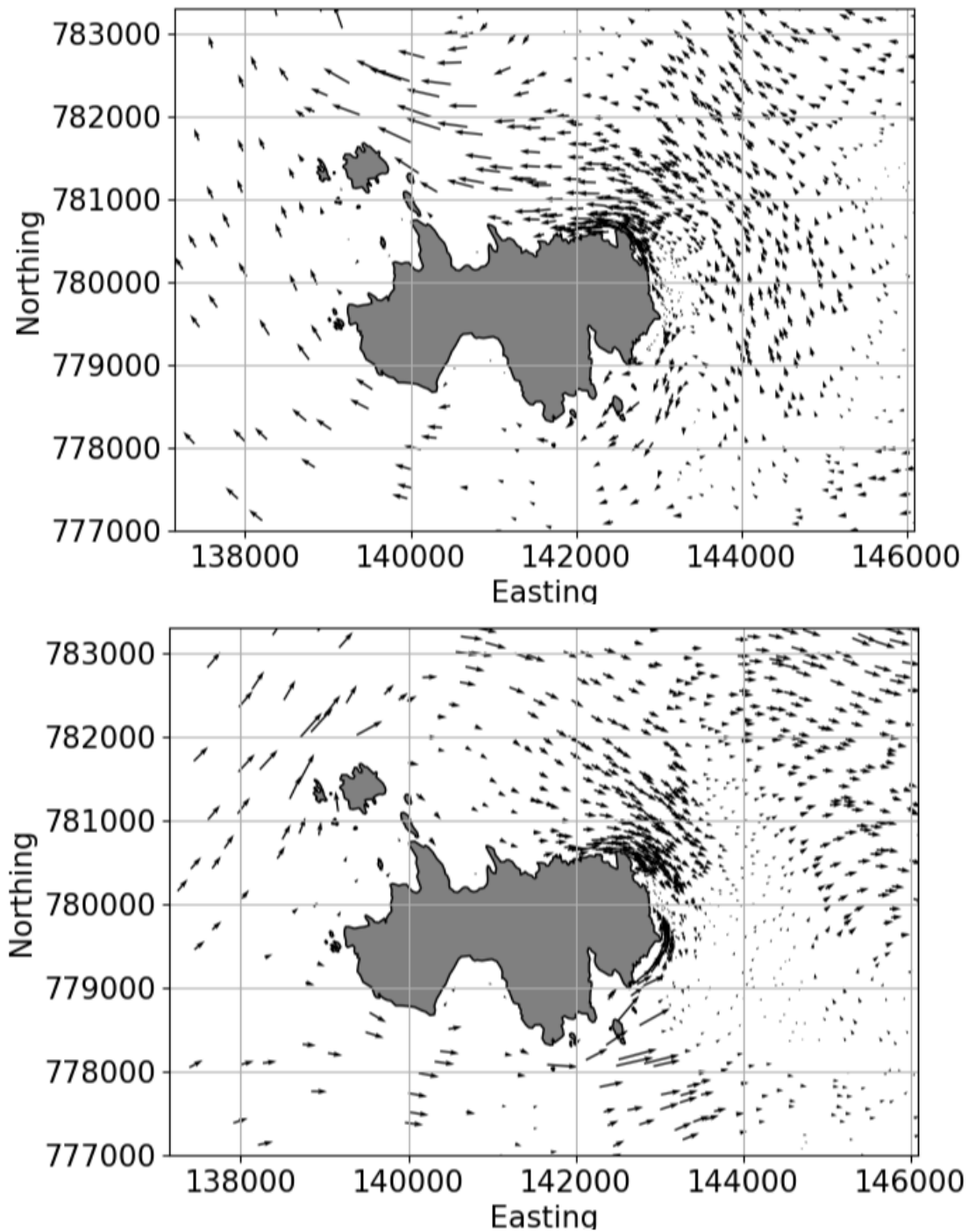
5. References and Bibliography

Casulli, V. 1987. Eulerian-lagrangian methods for hyperbolic and convection dominated parabolic problems. In: Taylor, C., Owen, D., Hinton, E. (Eds.), Computational Methods for Non-linear Problems, Pineridge Press, Swansea,U.K., pp. 239–268.

European Marine Observation and Data Network (EMODnet), 2022 Bathymetry | European Marine Observation and Data Network (EMODnet)

European Centre for Medium-Range Weather Forecasts (ECMWF) 2021, ERA5 Dataset https://www.ecmwf.int/en/forecasts/datasets/reanalysis-datasets/era5

Gillibrand, P.A.; Lane, E.M.; Walters, R.A.; Gorman, R.M. 2011. Forecasting extreme sea surface height and coastal inundation from tides, surge and wave setup. Austr. J. Civil Eng. 9, 99-112.

Gillibrand, P.A., Walters, R.A., and McIlvenny, J., 2016. Numerical simulations of the effects of a tidal turbine array on near-bed velocity and local bed shear stress. *Energies*, vol 9, no. 10, pp. 852. DOI: 10.3390/en9100852

Lane, E.M.; Gillibrand, P.A.; Arnold, J.R.; Walters, R.A. 2011. Tsunami inundation modeling with RiCOM. Austr. J. Civil Eng., 9, 83-98.

Large. W.G. and Pond, S., 1981. Open ocean momentum flux measurements in moderate to strong winds. J. Phys. Oceanogr., 11, 324—336.

Marine Scotland, 2016. Scottish Shelf Model. Part 1: Shelf-Wide Domain. Available at https://data.marine.gov.scot/dataset/scottish-shelf-model-part-1-shelf-wide-domain

McIlvenny, J. , Tamsett, D., Gillibrand, P.A. and Goddijn-Murphy, L., 2016. Sediment Dynamics in a Tidally Energetic Channel: The Inner Sound, Northern Scotland. Journal of Marine Science and Engineering, 4, 31; doi:10.3390/jmse4020031

Mowi Scotland Ltd, 2022. Muck Azamethiphos Dispersion Modelling Report. February 2022.

Plew, D. R.; Stevens, C. L. 2013. Numerical modelling of the effect of turbines on currents in a tidal channel–Tory Channel, New Zealand. Renew. Energy, 57, 269-282.

Walters, R. A. 2005a. Coastal ocean models: two useful finite element methods. Cont. Shelf Res., 25(7), 775-793.

Walters, R. A. 2005b. A semi-implicit finite element model for non-hydrostatic (dispersive) surface waves. Int. J. Num. Meth. Fluids, 49(7), 721-737.

Walters, R.A. 2016. A coastal ocean model with subgrid approximation. *Ocean Mod.*, 102, 45-54.

Walters, R.A.; Casulli, V., 1998. A robust, finite element model for hydrostatic surface water flows. Comm. Num. Methods Eng., 14, 931–940.

Walters, R.A.; Gillibrand, P.A.; Bell, R.; Lane, E.M. 2010. A Study of Tides and Currents in Cook Strait, New Zealand. Ocean Dyn., 60, 1559-1580.

Walters, R.A., Lane, E.M., Hanert, E. 2009. Useful time-stepping methods for the Coriolis term in a shallow water model. *Ocean Model.*, *28*, 66–74. doi: 10.1016/j. ocemod.20 08.10.0 04.

Walters, R.A. ; Lane, E.M.; Henry, R.F. 2008. Semi-lagrangian methods for a finite element coastal ocean model. *Ocean Model.*, 19, 112–124.

Walters, R. A.; Tarbotton, M. R.; Hiles, C. E. 2013. Estimation of tidal power potential. Renew. Energy, 51, 255-262.

Willmott, C. J.; Ackleson, S. G.; Davis, R. E.; Feddema, J. J.; Klink, K. M.; Legates, D. R. O'Donnell, J.; Rowe, C. M. 1985. Statistics for evaluation and comparison of models, J. Geophys. Res., 90, 8995– 9005.

Wu, J. 1982. Wind-stress coefficients over sea surface from breeze to hurricane, J. Geophys. Res., 87(C12), 9704–9706, doi:10.1029/JC087iC12p09704.